A GRATING-BASED PLASMON BIOSENSOR WITH HIGH RESOLUTION

Z. Luo[1, *], T. Suyama[1], X. Xu[2], and Y. Okuno[1]

[1]Graduate School of Science and Technology, Kumamoto University, Kumamoto 860-8555, Japan

[2]Department of Electrical Engineering and Information Technology, Kyushu Sangyo University, Fukuoka 813-8503, Japan

Abstract—We present an idea of grating-based plasmon biosensor utilizing phase detection to realize high resolution in finding a refractive index of a material put on the surface of a metal grating. Considering a trade-off between high resolution and experimental practicability, we show a table of recommended setup that covers a wide range of the index. Keeping the diffraction efficiency no less than 10^{-3} and assuming the resolution in phase detection to be 2.5×10^{-2} degrees, we estimate the resolution of the biosensor as 7.5×10^{-7} refractive index units. We also discuss the possible improvement to realize a predicted superior limit of resolution around 10^{-8} refractive index units.

1. INTRODUCTION

A metal grating has an interesting property known as the resonance absorption [1]: partial or total absorption of incident light energy occurs at a specific angle of incidence (resonance angle). This is caused by excitation of plasmon surface waves and is accompanied by an abrupt change of diffraction efficiency [1–5]. For a grating placed in planer mounting ($\varphi = 0°$ in Fig. 1) the excitation can be seen in TM incidence alone. While in conical mounting ($\varphi \neq 0°$) this occurs in both TM and TE incidence.

We know that the resonance absorption occurs when a phase-matching condition is satisfied: the phase constant of an evanescent order coincides with the real part of an eigenvalue of surface plasmons. This means that the resonance angle is determined by the grating
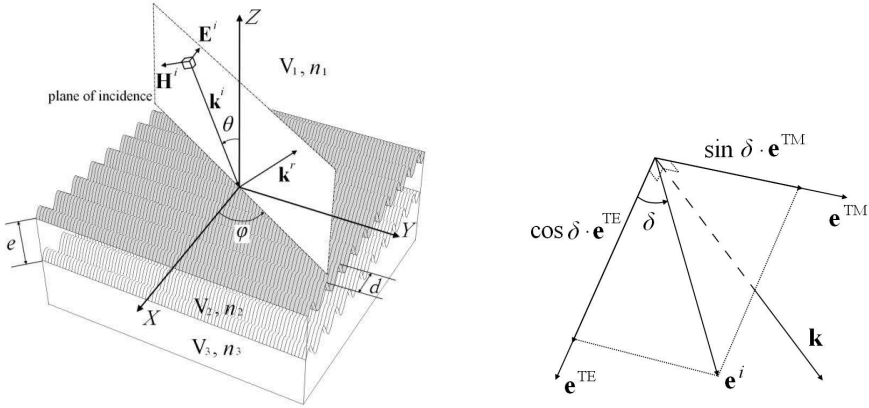
Figure 1. Schematic representation of diffraction by a layered metal grating and definition of the polarization angle.

parameters, the incident wave, and the refractive index of a material over the grating surface. Hence, if we measure the resonance angle by observing the TM-wave efficiency, we can find the index of the material by making comparison with results of computer simulation. This is a grating-based plasmon index sensor or a biosensor.

According to our prevenient research, we can easily determine the refractive index of the material with an accuracy of five digits by measuring the zeroth-order efficiency alone [6]. The five-digit resolution, however, is not sufficient for practical applications, for example, in clinical medicine or physiology where a 7-digit resolution is usually required [7, 8]. Hence, we have an urgent issue to increase the resolution in the index determination.

A promising solution to our issue is to employ phase detection to measure the phase modulation accompanying the plasmon excitation. This is because the Fresnel models of surface plasmon excitation predict an obvious change in the reflected phase as the material index changed [7]. The phase detection has already been employed in prism-based biosensors and works to improve the resolution of the sensors to 10^{-7} refractive index units (RIU) [7, 9–11].

In the following sections we examine the possibility of the phase detection employed in the grating-based plasmon biosensor. In Section 2, we will formulate the problem of diffraction by a metal grating placed in conical mounting and describe the method of solution employed [12, 13]. In Section 3, we will show the numerical results and will make discussions from the viewpoint of sensor applications.

2. FORMULATION OF THE PROBLEM AND THE METHOD OF SOLUTION

2.1. Statement of the Problem

Figure 1 shows the schematic representation of diffraction by a layered grating made of a metal and having an over-coating made of another metal. The grating is uniform in the Y direction and is periodic in X. The surface profiles are given by

$$S_1 : \ z_1 = \eta_1(x) = h \sin(2\pi x/d) \tag{1a}$$
$$S_2 : \ z_2 = \eta_2(x) = h \sin(2\pi x/d) - e \tag{1b}$$

where h, d, and e are the amplitude (half depth) of the surface modulation, the period, and the thickness of the coating. Note that the small letters (x, y, z) denote a point on the surfaces.

The surfaces separate the whole space into three regions:

$$\begin{aligned} V_1 : \ & Z > \eta_1(X) \\ V_2 : \ & \eta_1(X) > Z > \eta_2(X) \\ V_3 : \ & \eta_2(X) > Z \end{aligned} \tag{2}$$

We assume that V_1, V_2, and V_3, respectively, are filled with a dielectric (with a positive refractive index n_1), a metal (having a complex-valued index n_2), and another metal (with n_3). The capital letters (X, Y, Z) show the coordinates of a point in these regions. A convention $\mathbf{P} = (X, Y, Z)$ will be used as well.

The electric field of an incident light is given by

$$\mathbf{E}^i(\mathbf{P}) = \mathbf{e}^i \exp\left(i\mathbf{k}^i \cdot \mathbf{P} - i\omega t\right) \tag{3}$$

where

$$\mathbf{k}^i = (\alpha, \beta, -\gamma) \tag{4}$$

with $\alpha = n_1 k^i \sin\theta \cos\phi$, $\beta = n_1 k^i \sin\theta \sin\phi$, $\gamma = n_1 k^i \cos\theta$, and $k^i = 2\pi/\lambda$. As shown in Fig. 1, θ is the polar angle between the Z-axis and the incident wave-vector, φ is the azimuth angle between the X-axis and the plane of incidence, and λ is the wavelength in vacuum.

When $\varphi = 0°$, the incident light comes from a direction orthogonal to the grooves and the diffracted waves propagate in directions in the plane of incidence. This arrangement is called the *planer mounting* (or classical mounting). While if $\varphi \neq 0°$, as shown in Fig. 1, the directions lie on a cone centered at the origin. This is termed the *conical mounting*.

Let us decompose the amplitude $\mathbf{e}^i$ appeared in (3) into a TE- and a TM-component, where TE (or TM) means the absence of the

Z-component in the relevant electric (or magnetic) field. To do this, we first define two unit vectors that span a plane orthogonal to $\mathbf{k}^i$:

$$\mathbf{e}^{\mathrm{TE}} = (\sin\varphi, \ -\cos\varphi, \ 0) \tag{5a}$$

$$\mathbf{e}^{\mathrm{TM}} = (\cos\theta\cos\varphi, \ \cos\theta\sin\varphi, \ \sin\theta) \tag{5b}$$

Apparently, $\mathbf{e}^{\mathrm{TE}}$ has no *Z*-component. The fact that the magnetic amplitude accompanying $\mathbf{e}^{\mathrm{TM}}$ cannot have any *Z*-component is seen by direct manipulation. In addition, they are perpendicular to each other, and both of them make a right angle with $\mathbf{k}^i$. Hence, they are the unit vectors in the direction of the TE- and TM-component in the sense above. The amplitude $\mathbf{e}^i$ is decomposed as

$$\mathbf{e}^i = \mathbf{e}^{\mathrm{TE}}\cos\delta + \mathbf{e}^{\mathrm{TM}}\sin\delta \tag{6}$$

where δ, which is termed a polarization angle, is the angle between $\mathbf{e}^{\mathrm{TE}}$ and $\mathbf{e}^i$ (see Fig. 1). In particular, $\delta = 0°$ means TE incidence and $\delta = 90°$ stands for TM incidence. Thus the incident light is specified by the wavelength λ, the polar angle θ, the azimuth angle φ, and the polarization angle δ.

We consider the problem to seek the diffracted electric and magnetic fields in V_j $(j = 1, 2, 3)$. Note that they consist of both TE- and TM-components because we assume the conical mounting. The solutions should satisfy the following requirements:

(D1) the Helmholtz equations in each region;

(D2) a radiation condition in the *Z*-direction that the diffracted waves in V_1 (or V_3) propagate or attenuate in positive (or negative) *Z* direction;

(D3) a periodicity condition that the relation $f(X + d, Y, Z) = \exp(i\alpha d) f(X, Y, Z)$ holds and the phase constant in Y is β for any component of diffracted light;

(D4) the boundary conditions on S_1 and S_2 that the tangential components of the electric and magnetic fields must be continuous across the boundary.

2.2. Method of Solution

Because the diffracted fields have both TE- and TM-components, we need TE and TM vector modal functions to construct the solutions. The modal functions are derived from the Floquet modes (separated solutions of the Helmholtz equation satisfying the periodicity condition; and the radiation condition if necessary) and are defined by

$$\boldsymbol{\varphi}_{jm}^Q\left(\vec{P}\right) = \mathbf{e}_{jm}^Q \exp\left(i\mathbf{k}_{jm}\cdot\mathbf{P}\right) \tag{7}$$

for $Q = \text{TE, TM}$; $j = 1, 2, 3$; $m = 0, \pm 1, \pm 2 \ldots$. Here, the unit vectors in (7) are defined by

$$\mathbf{e}_{jm}^{\text{TE}} = \mathbf{k}_{jm} \times \mathbf{i}_Z / |\mathbf{k}_{jm} \times \mathbf{i}_Z| \tag{8a}$$

$$\mathbf{e}_{jm}^{\text{TM}} = \mathbf{e}_{jm}^{\text{TE}} \times \mathbf{k}_{jm} / \left| \mathbf{e}_{jm}^{\text{TE}} \times \mathbf{k}_{jm} \right| \tag{8b}$$

and

$$\mathbf{k}_{1m} = (\alpha_m, \ \beta, \ \gamma_{1m}) \tag{9a}$$

$$\mathbf{k}_{2m} = (\alpha_m, \ \beta, \ -\gamma_{2m}) \tag{9b}$$

$$\mathbf{k}_{3m} = (\alpha_m, \ \beta, \ -\gamma_{3m}) \tag{9c}$$

with

$$\alpha_m = \alpha + 2m\pi/d \tag{10}$$

and

$$\gamma_{jm}^2 = (n_j k)^2 - \left(\alpha_m^2 + \beta^2 \right) \tag{11}$$

Note that the modal functions given in (7) are used to construct diffracted electric fields. For the magnetic fields, the modal function can be obtained from (7) though Maxwell's equations as:

$$\boldsymbol{\psi}_{jm}^Q (\mathbf{P}) = \mathbf{k}_{jm} \times \boldsymbol{\varphi}_{jm}^Q (\mathbf{P}) / (\omega \mu_0) \tag{12}$$

Note further that the approximate solutions in V_1 are defined as finite linear combinations of up-going modal functions with unknown modal coefficients. Likewise, the solutions in V_3 are finite sums of down-going modal functions. However, the solutions in V_2 must have both up- and down-going modal functions. To distinguish the traveling direction of a modal function in each region, we use superscripts $+$ and $-$ representing up- and down-going waves. All the solutions, of course, should consist of TE- and TM-components unless $\varphi = 0$ (planer-mounting case).

The approximate solutions in each region, hence, can be expressed as:

$$\begin{pmatrix} \mathbf{E}_{1N}^d \\ \mathbf{H}_{1N}^d \end{pmatrix}(\mathbf{P}) = \sum_{n=-N}^{N} A_{1n}^{\text{TE}+}(N) \begin{pmatrix} \phi_{1n}^{\text{TE}+} \\ \varphi_{1n}^{\text{TE}+} \end{pmatrix}(\mathbf{P}) + \sum_{n=-N}^{N} A_{1n}^{\text{TM}+}(N) \begin{pmatrix} \phi_{1n}^{\text{TM}+} \\ \varphi_{1n}^{\text{TM}+} \end{pmatrix}(\mathbf{P})$$

$$\begin{pmatrix} \mathbf{E}_{2N}^d \\ \mathbf{H}_{2N}^d \end{pmatrix}(\mathbf{P}) = \sum_{n=-N}^{N} A_{2n}^{\text{TE}-}(N) \begin{pmatrix} \phi_{2n}^{\text{TE}-} \\ \varphi_{2n}^{\text{TE}-} \end{pmatrix}(\mathbf{P}) + \sum_{n=-N}^{N} A_{2n}^{\text{TM}-}(N) \begin{pmatrix} \phi_{2n}^{\text{TM}-} \\ \varphi_{2n}^{\text{TM}-} \end{pmatrix}(\mathbf{P})$$

$$+ \sum_{n=-N}^{N} A_{2n}^{\text{TE}+}(N) \begin{pmatrix} \phi_{2n}^{\text{TE}+} \\ \varphi_{2n}^{\text{TE}+} \end{pmatrix}(\mathbf{P}) + \sum_{n=-N}^{N} A_{2n}^{\text{TM}+}(N) \begin{pmatrix} \phi_{2n}^{\text{TM}+} \\ \varphi_{2n}^{\text{TM}+} \end{pmatrix}(\mathbf{P})$$

$$\begin{pmatrix} \mathbf{E}_{3N}^d \\ \mathbf{H}_{3N}^d \end{pmatrix}(\mathbf{P}) = \sum_{n=-N}^{N} A_{3n}^{\text{TE}-}(N) \begin{pmatrix} \phi_{3n}^{\text{TE}-} \\ \varphi_{3n}^{\text{TE}-} \end{pmatrix}(\mathbf{P}) + \sum_{n=-N}^{N} A_{3n}^{\text{TM}-}(N) \begin{pmatrix} \phi_{3n}^{\text{TM}-} \\ \varphi_{3n}^{\text{TM}-} \end{pmatrix}(\mathbf{P})$$

$$\tag{13}$$

where N is the number of truncation. Since the approximate solutions satisfy the requirements (D1), (D2), and (D3), the modal coefficients should be determined in order that the solutions satisfy the boundary condition (D4) in an approximate sense. According to Yasuura's theory [12], we determine the coefficients by the least-squares method.

In (13), we see that there are 8 $(2N + 1)$ unknown coefficients in total. It is known that the sufficient number of equations in the least-squares approximation is twice as many as the number of unknowns [13]. Hence, locating $J = 2(2N + 1)$ equally-spaced sampling points on one period of both S_1 and S_2 and describing the boundary conditions at these points, we have $16(2N + 1)$ linear equations for the coefficients. This over-determined set of equations is solved approximately by the QR-decomposition.

3. NUMERICAL RESULTS AND DISCUSSION

In this section, we show numerical results obtained by the method above and discuss the possibility of high resolution.

3.1. Preparation for Calculation

In the following, we assume the use of a commercial grating made of aluminum with an gold over-coating, whose parameters are $2h = 0.072\,\mu$m, $d = 0.556\,\mu$m and $e = 0.778\,\mu$m. The incident light is a monochromatic plane wave from a laser diode with a wavelength of $0.633\,\mu$m. As for the value taken in our computation, we assume that the refractive indices of Al and Au at this wavelength are $n_2 = 0.1594 + i3.2166$ and $n_3 = 1.2078 + i7.0148$ [14]. However, it should be noted that the index of a metal film depends not only on the wavelength but also on the thickness of the film when the film is extremely thin. It may take unusual values if circumstances require. When dealing with a thin metal structure, hence, we should be careful in using the index value given in the literature.

The efficiency of the zeroth-order TM diffracted mode in V_1 is defined as the per period power carried away by the zeroth mode normalized by the per period incident power, the efficiency of the zeroth-order TM mode is then given by

$$\rho_0^{\mathrm{TM}} = (\gamma_0/\gamma) \left| A_0^{\mathrm{TM}} \right|^2 \qquad (14)$$

3.2. Numerical Results

Figure 2 shows the efficiency of TM_0 mode as a function of the incident polar angle θ for different azimuth angles while V_1 is filled with a

dielectric of refractive index $n_1 = 1.330$. Each curve in the figure shows a resonant incident polar angle θ for a given azimuth angle.

Correspondingly, Fig. 3 shows the phase shift of TM_0 mode while the refractive index n_1 changes around 1.330. The phase shift curve has a steep slope over a limited range of refractive index. We also notice that the slopes of phase shift curves are related with the strength of the resonance absorption. That is, the strongest resonance with almost total absorption observed at $\theta = 20.5°$ and $\varphi = 11.2°$ is accompanied with the most abrupt slope of the phase shift curve.

Figure 3 shows greater potential of a grating-based biosensor with phase detection than one with efficiency-alone measurement for the purpose of high resolution. In an experimental design, the light from a light source is first separated into a signal and a reference beam. The former illuminates the grating through a material with an index n_1 and a part of the incident power is reflected after exciting the plasmon surface wave. Note that the phase of the reflected beam is modulated and the magnitude of the modulation depends on n_1 as we have seen above. Comparison of the phase of the modulated signal beam with that of the reference beam finds the phase shift caused by the resonance absorption, the phase shift which is on the ordinate of Fig. 3. As a result, the refractive index of the material over the grating surface can be accurately determined by the curve.

Obviously, the resolution of such a sensor design is related to the slope of a curve chosen from the curves in Fig. 3. Although a steeper slope means higher resolution, the steepest curve in Fig. 3 ($\theta = 20.5°$ and $\varphi = 11.2°$) is difficult to be employed in practice because of an extremely low efficiency far less than 10^{-3}. We, hence, have to consider the optical setting in accordance with experimental limits.

Combining Figs. 2 and 3, we find the setting that causes the highest resolution also shows the lowest reflection intensity in the simulation parameters that we have assumed. Depending on the amplitude sensitivity of photo-detectors, the diffraction efficiency of the zeroth-order TM wave should have a lower limit. Therefore, we have a trade-off between high resolution and a sufficient diffracted power. For example, we can choose the secondary tilted current ($\theta = 20.3°$ and $\varphi = 5.6°$) in experiment to ensure that the signal beam is strong enough to be detected. If we choose these parameters, and if we refer to an experimental design whose instrumental resolution in phase detection is 2.5×10^{-2} degrees [15], then we can expect the resolution in refractive index should be about 7.5×10^{-7} RIU.

Next, we move on to another issue of extending the measurement range. Because the magnitude of a phase shift cannot be more than $180°$, high resolution (i.e., the steep curves in Fig. 3) means a narrow
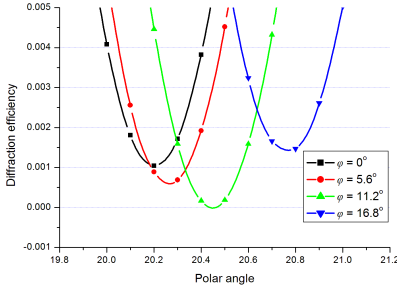
Figure 2. Diffraction efficiency as a function of polar angle for given azimuth angles.
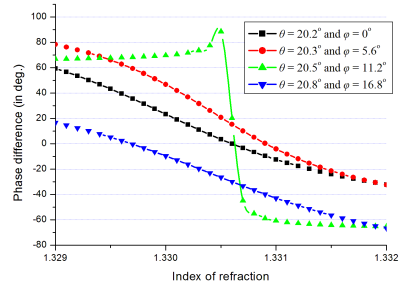
Figure 3. Phase response for different incident angles.

Table 1. Workspaces and recommended settings for polar angle θ and azimuth angle φ.

Workspace (index range)	θ	φ	Workspace (index range)	θ	φ
$1.271 \sim 1.274$	$15.6°$	$6.4°$	$1.329 \sim 1.332$	$20.3°$	$5.6°$
$1.274 \sim 1.277$	$15.8°$	$6.5°$	$1.332 \sim 1.335$	$20.5°$	$5.7°$
$1.277 \sim 1.280$	$16.0°$	$6.4°$	$1.335 \sim 1.338$	$20.7°$	$5.6°$
$1.280 \sim 1.283$	$16.3°$	$6.4°$	$1.338 \sim 1.341$	$21.0°$	$5.5°$
$1.283 \sim 1.286$	$16.5°$	$6.4°$	$1.341 \sim 1.344$	$21.2°$	$5.5°$
$1.286 \sim 1.289$	$16.8°$	$6.3°$	$1.344 \sim 1.347$	$21.4°$	$5.4°$

measurement range in refractive index. For example, a setting with $\theta = 20.5°$, $\varphi = 5.6°$ is available in a range $1.329 < n_1 < 1.332$, which will be called a workspace below. Table 1 shows an example of recommended settings for an index range $1.271 < n_1 < 1.347$ obtained through a systematic computer simulation, the settings which keep the efficiency no less than 10^{-3} and remain $100°$ phase shift throughout corresponding workspaces. This means the expected resolution in n_1, again, is 7.5×10^{-7} throughout the table. With such a range, this index determination method can fit a metal grating to measure refractive indices of either gas or liquid samples.

We observe in this table that the workspace can be shifted from low to high index range by increasing the polar angle θ. It is worth noting that for a fixed polar angle, the resonance moves also from low to high index along with decrease of the azimuth angle φ. By setting the incident angles properly, the strength of the absorption and the

extent of the workspace, which is related to the resolution, can be controlled.

3.3. Deeper Discussion

High resolution is the main aim that we are pursuing. To achieve the aim we employed the phase detection of the zeroth-order diffracted TM mode and faced a trade-off between the resolution and the sensitivity of a detector. This was because the steepest curve in Fig. 3 corresponds to the almost total absorption in Fig. 2 and the TM component of the diffracted beam cannot be detected. One may doubt why we do not observe the TE_0 component because it does not couple with the plasmons and the efficiency in the TE mode should be much greater than that of the TM mode. Although the prediction of the greater efficiency is usually correct, we cannot employ the phase modulation of the TE mode. This is because the TE components have been excited just to fit the boundary conditions in the conical mounting but not to participate in the resonance absorption. In fact, in our simulation results, the phase of the TE_0 component floats no more than 1 or 2 degrees within a large refractive index range. Thus, it is quite difficult to pick up useful information from the phase of the TE_0 component. In practical experiments, we employ a phase detection scheme using a photo-elastic modulator (PEM) [16, 17], for example, in which the signal from the PEM is stable enough as a reference in phase modulation measurement.

Next, let us consider a superior limit of resolution assuming the use of the steepest curve in Fig. 3 ($\theta = 17.2°$ and $\varphi = 12.6°$). Although this setting is not practical under the assumptions in this work, we mention the limit because there are a couple of possible ways to avoid the experimental problem. For example:
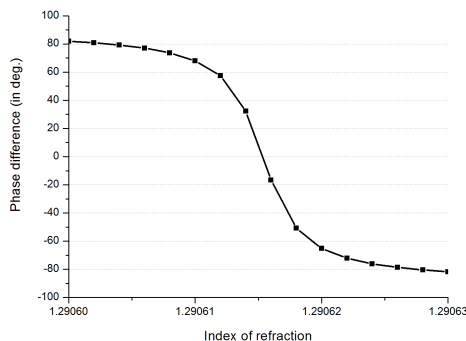
Figure 4. Phase response for $\theta = 17.2°$, $\varphi = 12.6°$.

(1) By modifying the grating shape, we can control the TM_0 efficiency to get a sufficient power in the TM_0 reflected beam;

(2) By using the coupling of the second-order evanescent mode and observing the zeroth- and the first-order diffracted TM mode, we have a chance to get sufficient power for phase detection;

(3) Technical development may allow us to detect the phase of an extremely small signal beam.

Even in the case if (1), (2), or (3) works successfully, we think that the practical limit of resolution cannot exceed one predicted from the steepest curve. Fig. 4 is a magnification of the curve with the most

Table 2. Workspaces and recommended settings for polar angle θ and azimuth angle φ.

Workspace (index range)	θ	φ	Phase shift
$1.2705 \sim 1.2710$	$15.6°$	$13.0°$	$155°$
$1.2710 \sim 1.2715$	$15.6°$	$12.4°$	$105°$
$1.2715 \sim 1.2720$	$15.7°$	$13.4°$	$129°$
$1.2720 \sim 1.2725$	$15.7°$	$13.0°$	$151°$
· · · · · ·			
$1.2890 \sim 1.2895$	$17.1°$	$12.6°$	$176°$
$1.2895 \sim 1.2900$	$17.1°$	$12.2°$	$121°$
$1.2900 \sim 1.2905$	$17.2°$	$13.1°$	$119°$
$1.2905 \sim 1.2910$	$17.2°$	$12.6°$	$178°$
· · · · · ·			
$1.3230 \sim 1.3235$	$19.9°$	$11.8°$	$140°$
$1.3235 \sim 1.3240$	$19.9°$	$11.1°$	$118°$
$1.3240 \sim 1.3245$	$20.0°$	$11.9°$	$135°$
$1.3245 \sim 1.3250$	$20.0°$	$11.4°$	$149°$
· · · · · ·			
$1.3305 \sim 1.3310$	$20.5°$	$11.2°$	$148°$
$1.3310 \sim 1.3315$	$20.5°$	$10.5°$	$112°$
$1.3315 \sim 1.3320$	$20.6°$	$11.2°$	$130°$
$1.3320 \sim 1.3325$	$20.6°$	$10.7°$	$147°$
· · · · · ·			
$1.3400 \sim 1.3405$	$21.3°$	$10.8°$	$143°$
· · · · · ·			

obvious slope in our simulation works. We observe a steep slope over a limited range of n_1 from 1.29061 to 1.29062, which is the workspace defined by the parameters $\theta = 17.2°$ and $\varphi = 12.6°$. The phase shift in this workspace is 176 degrees and we predict the resolution to be 10^{-9} RIU.

Strong resonance absorption similar to above also occurs for different values of n_1 provided that the polar and azimuth angle are chosen appropriately. Table 2 shows examples of recommended angles for each workspace having a common width of 0.0005 RIU. In each workspace the phase shift is more than $100°$, which is needed to keep a 5×10^{-8} RIU resolution while the smallest efficiency is no less than 10^{-7}.

4. CONCLUSION

Since the sample index n_1 has large influence on the phase modulation of the diffracted TM mode, the phase detection is a strong way to find the index. The resolution of the possible grating-based biosensor with phase detection will be 7.5×10^{-7} RIU in the state-of-the-art today. This means more than 7-digit determination of the index and can be employed for medical and physiological applications.

In addition, we made discussion on the possibility of achieving higher resolution and stated that the superior limit should be 10^{-9} RIU. Because the light velocity in vacuum is a constant having 9 significant figures, this limit is more than enough. Hence, a grating-based biosensor with phase detection has potential in determining the index to any accuracy having physical meaning.

So far we have indicated a possible system with ultrahigh resolution and measurement of relative values of refraction. Of course in achieving such ultrahigh resolution to measure precisely an absolute value of refractive index of environment medium, we should control every factor in experimental environment precisely: the grating parameters including the indices n_2 and n_3, the angles of incidence, the wavelength, the room temperature, and so on. Because the refractive index of a metal, in particular, if it is a thin film, is not easy to be determined, it is worth to note that we can find the indices n_2 and n_3 by comparing the experimental data with simulation results [18] provided the other parameters are sufficiently correct. In addition, some other phenomena, such as rotation of polarization caused by optically active molecules, birefringence or double refraction seen in anisotropic media, etc., are possible factors that may affect the performance in high resolution. We would like to examine these issues in our future works towards realization of ultrahigh resolution.

ACKNOWLEDGMENT

REFERENCES

1. Raeter, H., "Surface plasmon and roughness," *Surface Polaritons*, V. M. Argranovich and D. L. Mills (eds.), Ch. 9, 331–403, North-Holland, New York, 1982.

2. Nevière, M., "The homogeneous problem," *Electromagnetic Theory of Gratings*, R. Petit, Ed., 123–157, Springer-Verlag, Berlin, 1980.

3. Barnes, W. L., T. W. Preist, J. R. Sambles, N. P. K. Cotter, and D. J. Nash, "Photonic gaps in the dispersion of surface plasmons on gratings," *Phys. Rev. B*, Vol. 51, 11164–11167, 1995.

4. Chau, Y.-F., H.-H. Yeh, and D. P. Tsai, "Surface plasmon resonances effects on different patterns of solid-silver and silvershell nanocylindrical pairs," *Journal of Electromagnetic Waves and Applications*, Vol. 24, Nos. 8–9, 1005–1014, 2010.

5. Zhao, J., K. Li, F.-M. Kong, and L.-G. Du, "Enhancement of blue light emission using surface plasmons coupling with quantum wells," *Progress In Electromagnetics Research*, Vol. 108, 293–306, 2010.

6. Suyama, T. and Y. Okuno, "Enhancement of TM-TE mode conversion caused by excitation of surface plasmons on a metal grating and its application for refractive index measurement," *Progress In Electromagnetics Research*, Vol. 72, 91–103, 2007.

7. Nelson, S. G., K. S. Johnston, and S. S. Yee, "High sensitivity surface plasmon resonance sensor based on phase detection," *Sensors and Actuators B*, Vol. 35, Issues 1–3, 187–191, 1996.

8. Banerjee, A., "Enhanced refractometric optical sensing by using one-dimensional ternary photonic crystals," *Progress In Electromagnetics Research*, Vol. 89, 11–22, 2009.

9. Ho, H. P., W. C. Law, S. Y. Wu, C. Lin, and S. K. Kong, "Real-time optical biosensor based on differential phase measurement of surface plasmon resonance," *Biosensors and Bioelectronics*, Vol. 20, 2177–2180, 2005.

10. Ho, H. P., W. Yuan, C. L. Wong, S. Y. Wu, Y. K. Suen, S. K. Kong, and C. Lin, "Sensitivity enhancement based on

application of multi-pass interferometry in phase-sensitive surface plasmon resonance biosensor," *Optics Communications*, Vol. 275, 491–496, 2007.

11. Wong, C. L., H. P. Ho, Y. K. Suen, S. K. Kong, Q. L. Chen, W. Yuan, and S. Y. Wu, "Real-time protein biosensor arrays based on surface plasmon resonance differential phase imaging," *Biosensors and Bioelectronics*, Vol. 24, 606–612, 2008.

12. Yasuura, K. and T. Itakura, "Approximation method for wave functions (I), (II) and (III)," *Kyushu Univ. Tech. Rep.*, Vol. 38, No. 1, 72–77, 1965; Vol. 38, No. 4, 378–385, 1966; Vol. 39, No. 1, 51–56, 1966.

13. Okuno, Y. and H. Ikuno, "Yasuura's method, its relation to the fictitious source methods, and its advancements in solving 2-D problems," *Generalized Multipole Techniques for Electromagnetic and Light Scattering*, T. Wriedt (ed.), 111–141, Elsevier, Amsterdam, 1999.

14. Hass, G. and L. Hadley, "Optical properties of metals," *American Institute of Physics Handbook*, 2nd editon, D. E. Gray (ed.), 6–107, McGraw-Hill, New York, 1963.

15. Horowitz, P. and W. Hill, *The Art of Electronics*, 641–646, Cambridge University Press, Cambridge, 1989.

16. Markowicz, P. P., W. C. Law, A. Baev, P. Prasad, S. Patskovsky, and A. V. Kabashin, "Phase-sensitive timemodulated SPR polarimetry for wide dynamic range biosensing," *Opt. Express*, Vol. 15, 1745, 2007.

17. Law, W.-C., P. Markowicz, K.-T. Yong, I. Roy, A. Baev, S. Patskovsky, A. V. Kabashin, H. P. Ho, and P. N. Prasad, "Wide dynamic range phase-sensitive surface plasmon resonance biosensor based on measuring the modulation harmonics," *Biosens. Bioelectron*, Vol. 23, No. 5, 627–632, 2007.

18. Okuno, Y. and T. Suyama, "Numerical analysis of surface plasmons excited on a thin metal grating," *Journal of Zhejiang University SCIENCE A*, Vol. 7, No. 1, 55–70, 2006.